Brain activity modeling in general anesthesia: Enhancing local mean-field models using a slow adaptive firing rate.

Behnam Molaee-Ardekani, Lotfi Senhadji, Mohammad Bagher Shamsollahi, Bijan Vosoughi-Vahdat, Eric Wodey

Brain Activity Modeling in General Anesthesia: Enhancing Local

Mean-Field Models Using a Slow Adaptive Firing Rate

B. Molaee-Ardekani[1,2,3], L. Senhadji[1,2*], M.B. Shamsollahi[3], B. Vosoughi-Vahdat[3], E. Wodey[1,2,4]

[1] INSERM, U 642, Rennes F-35000, France;

[2] Université de Rennes 1, LTSI, Rennes F-35000, France;

[3] BiSIPL, School of Electrical Engineering, Sharif University of Technology, Tehran, Iran;

[4] CHU de Rennes, Service d'Anesthésie Réanimation 2, Rennes F-35000, France.

behnam.molaee-ardekani@univ-rennes1.fr , b_molaee@mehr.sharif.edu , mbshams@sharif.edu

Abstract - In this paper, an enhanced local mean-field model that is suitable for simulating the electroencephalogram (EEG) in different depth of anesthesia is presented. The main building elements of the model (e.g. excitatory and inhibitory populations) are taken from Steyn-Ross *et al* (M. L. Steyn-Ross *et al.*, Phys Rev E Stat Nonlin Soft Matter Phys **64**, 011917 (2001), D. A. Steyn-Ross *et al.*, Phys Rev E Stat Nonlin Soft Matter Phys **64**, 011918 (2001)) and Bojak & Liley (I. Bojak, and D. T. Liley, Phys Rev E Stat Nonlin Soft Matter Phys **71**, 041902 (2005)) mean-field models and a new slow ionic mechanism is included in the main model.

Generally, in mean-field models, some sigmoid-shape functions determine firing rates of neural populations according to their mean membrane potentials. In the enhanced model, the sigmoid function corresponding to excitatory population is redefined to be also a function of the slow ionic mechanism. This modification adapts the firing rate of neural populations to slow ionic activities of the brain. When an anesthetic drug is administered, the slow mechanism may induce neural cells to alternate between two levels of activity referred to as up and down states. Basically, the frequency of up-down switching is in the delta band (0-4 Hz) and this is the main reason behind high amplitude, low frequency fluctuations of EEG signals in anesthesia.

Our analyses show that the enhanced model may have different working states driven by anesthetic drug concentration. The model is settled in the up state in waking period, it may switch to up and down states in moderate anesthesia while in deep anesthesia it remains in the down state.

* Corresponding author: Tel: (+33)223235577; Fax: (+33)223236917; email address: lotfi.senhadji@univ-rennes1.fr (L. Senhadji)

1   INTRODUCTION

In the last decade, many efforts have been done to build monitors dedicated to the estimation of the depth of anesthesia using EEG recording [1]. However, until now there is no universal monitor able to provide reliable results in all cases (*i.e.* drugs, patient dependencies, etc). Better understanding of underlying neuronal mechanisms of the EEG may improve the performance of monitoring methods. Therefore, a physiological-based model that explains the evolution of the EEG signal in different depth of anesthesia may bring new insights into the monitoring of the depth of anesthesia. Mean-Field (MF) models [2, 3] are good candidates for this purpose. They have neurophysiological and neuroanatomical foundations and are based on the concept of neural population which handles thousands of similar neurons in a single structure. They are able to reproduce EEG-like signals with a low computation cost by solving a set of coupled differential equations.

One of the best MF models which can reproduces various EEG rhythms is the Liley model [4, 5]. Steyn-Ross *et al* [6-8] and Bojak *et al* [9] have employed the Liley model in different ways to describe how and why the dominant rhythm of the EEG changes from beta and alpha rhythms to delta rhythm by administration of anesthetic drugs. They differently express certain parameters of the Liley model as functions of anesthetic drug concentration and reproduce EEG signals in various drug concentrations. Although these models describe the reason why anesthesia slows down EEG rhythms, they have some limitations that must be addressed gradually by better understanding of brain functioning under anesthesia.

It has been shown that there is a good compatibility between fluctuations of high amplitude delta waves and internal states of cortical cells [10, 11]. During anesthesia, neural cells alternate almost synchronously between firing and rest modes that are referred to as up and down states respectively. Because of synchronization of neurons, neural populations have two different firing modes. This means that populations switch to up and down states during anesthesia. In previous MF models, it is assumed that neural populations always fluctuate about single equilibrium points.

The main purpose of this study is to show how MF models may be enhanced by including a slow modulating mechanism that is responsible of switching the state of the model to up and down. Many mechanisms have been presented as responsible mechanisms for generating the up and down states [12-14]; however it is still unclear which mechanisms play most important roles, and how they can be represented using the mean-field paradigm. Since we are mostly interested in introducing the general concepts of up and down states and their switching in neural populations, an enhanced MF model that integrates a generic form of a slow modulating mechanism is

2

proposed. This mechanism acts as a representative for various types of slow ionic currents either generated in cortical or subcortical regions.

In the next section, a brief state of the art of MF models in anesthesia is reported. Section 3 introduces the proposed enhanced model. Section 4 mainly discusses methods for analyzing the enhanced model. Finally, behaviors of the enhanced MF model in various anesthetic drug concentrations are presented in sections 5.

2   BASICS OF EEG MODELING IN ANESTHESIA

To our knowledge, researches conducted by Steyn-Ross *et al* were the first attempts to explain, using an MF model, why gradual increase of anesthetic concentration produces a sudden transition between awareness and unconsciousness [6-8]. In their model, anesthetic agents prolong the decay time of $GABA_A$ receptors. Equilibrium solutions of the coupled differential equations in various drug concentrations make an S-bend with one unstable and two stable branches. According to Steyn-Ross *et al*, when anesthetic concentration is gradually increased or decreased, the equilibrium solution of the model suddenly jumps from one stable branch to another and this can cause sudden transition between awareness and unconsciousness. Since phase transitions make a hysteresis path, emergence and induction phases of anesthesia take place in different drug concentrations.

Steyn-Ross *et al* indicate that their model may simulate the biphasic response. Biphasic response is a kind of transient activation-depression of the EEG signal that occurs in induction and recovery phases of anesthesia [15]. Later, Bojak & Liley [9] modify the Steyn-Ross *et al* model. They develop better formulations to describe inhibitory and excitatory post synaptic potentials (IPSP/EPSP) in different anesthetic drug concentrations. Bojak & Liley also argue that anesthetic drugs reduce the firing rate of spontaneous action potentials in a relatively smooth dose-dependent manner and as a result, mean membrane potentials of inhibitory and excitatory populations do not change abruptly by increasing or decreasing anesthetic drug concentration. According to this statement, Bojak & Liley generate a large set of spectra and compare them to empirical EEG recordings using some classical features such as SEF_{90} (Spectral Edge Frequency defined as the frequency below which 90% of the power in the electroencephalogram resides). The biphasic response of the Bojak & Liley model is produced differently compared to that of the Steyn-Ross *et al* model. It takes place in the same drug concentration in induction and recovery phases (*i.e.* non-hysteresis path).

Our proposed enhanced MF model is mainly established on Steyn-Ross *et al* [6] and Bojak & Liley models [9]. A slow ionic mechanism is also incorporated in the model that let us to have a better justification of some neurophysiological phenomena. For example, this enhanced model may describe the reason for appearance of two different modes of neural firing rates and high amplitude delta waves observing in moderate to deep depth of

3

anesthesia.

Experimental observations show that anesthetic agents basically reduce the brain activity in a pulsating manner. Intra and extra cellular recordings during administration of many kinds of anesthetic drugs show that neurons are bi-stable and have short periods of firing separated by silence phases. During firing phases the firing rate is more or less equal to the firing rate of neurons in waking periods [16, 17]. Neural cells alternate between the firing phase (up state) and the silence phase (down state) almost synchronously. The result of this synchronous switching can be seen as high-energy slow waves. Figures 3 and 4 in [18] and figures 1 and 4 in [19] indicate that neural cells firings onsets correlate well with EEG slow waves. These waves are easily transferred in the brain media [20] and are recorded on the brain surface with high amplitudes. The enhanced MF model tries to take into account the above remarks by integrating a modulating slow mechanism to its basic foundation taken from the previous MF models.

In Appendix I, we have briefly introduced the basic eight differential equations of the enhanced model. They have been formed mainly by a combination of differential equations of the two previously mentioned well-known MF models. Figure 1 illustrates a schematic diagram of the enhanced model and its excitatory and inhibitory populations. The populations interact with each other by $GABA_A$ and AMPA receptors. According to the position of the indicated switch in Figure 1, the model may be set either to basic or enhanced mode. In the enhanced mode, the static firing rate function corresponding to the excitatory population is substituted with a slow dynamic firing rate mechanism (see section 3.3). This increases the number of coupled differential equations to nine.

Figure 1 around here.

3   ENHANCING MF MODELS IN ANESTHESIA

This section describes the physiological as well as the mathematical foundations of the enhanced model. Section 3.1 introduces the relation between up and down states in single neurons and neural populations. Slow modulating mechanisms that cause neural populations to switch to up and down states are discussed in section 3.2. Finally, the enhanced model equipped by a typical slow modulating mechanism is presented in section 3.3.

3.1   SINGLE NEURONS INDUCE UP/DOWN SATES IN CORTICAL NETWORKS

Experiments of Destexhe *et al* and Steriade *et al* indicate that the mean histogram of neural cells membrane potentials has two distinct peaks during anesthesia or non rapid eye movement (REM) sleep. One of them is centered in resting potential (*e.g.* –70 mV) and the other one in a higher potential (*e.g.* –57 mV) [11, 21, 22]. Existence of these two peaks on the histogram is an indication of two different states in neural cells.

Based on Fujisawa experiments [23], neural cells may have different patterns of firing, each one referred to as an internal state of neural cells. Fujisawa indicates that single neurons possess some internal firing states which are coherent in adjacent neurons. He declares that an internal state of single cells in a network represent the state of the network.

Destexhe *et al* and Steriade *et al* indicate that single neurons are in two different states (up and down) and Fujisawa shows that single neurons induce phase transitions of cortical networks with multiple internal states. Inferring from these works, the neural populations have also two states of electrical activities in anesthesia or non-REM sleep and it is one of the multiple internal states of neural populations. Comparisons of the pattern of neural firings in waking and anesthesia periods show that neurons change their internal states from continuous firing to phasic firing (bursts or spikes separated by silence phases) [10, 11]. Since phasic firing is almost synchronous in neural cells, the frequency of bursts or spikes appearances in single neurons determines the frequency of local field potentials.

The Liley MF model [5] has the capability of generating up and down states. For instance, the upper S-bend equilibrium branch of the Steyn-Ross *et al* model [6] can be related to up state because on the upper branch, populations have constantly high synaptic conductance and firing rates [21]. On the other hand, the lower S-bend equilibrium branch can be related to the down state. Establishing such relationships can justify the difference between synaptic conductance in the up and down states. It also describes the reason for recording of high amplitude EEG delta rhythm on brain surface during anesthesia. It seems likely that previous MF models encounter an inherent limitation in generating the slow and delta waves because they only consider either up or down state of neural populations in various anesthetic drug concentrations.

3.2   NEEDS TO INSERT SLOW IONIC MECHANISMS IN MF MODELS

As mentioned before, neurons have two different firing states in anesthesia. Synaptic receptors and ion-channels have different responses during each of these two firing states; therefore it is not only because of synaptic receptors that neural populations demonstrate two different firing states. A co-working between synapses and ionic mechanisms is responsible of generating up and down states. Neural firing patterns under different

anesthetic drugs are quite different [24] and it is mainly because of unique influences that each anesthetic drug has on synaptic [25-27] or ionic [28-31] mechanisms. As a result, simulating the effects of different anesthetic drugs on EEG signals is possible if ionic currents are also considered in MF models.

Different ionic mechanisms have been hypothesized for the slow switching of neural activities to up and down states. Compte et al [12] assert that existence of slow Na^+-dependent K^+ channels (I_{KNa}) on pyramidal cells (excitatory population) is mainly responsible for pulling down the state of neurons. Massimini and Amzica [13] state that during up state the gradual reduction of extra cellular Ca^{2+} concentration in response to high activity of synapses, or opening a kind of specific Ca^{2+} channel can produce a global dysfacilitation in cortical network that lead it to down state. Bazhenov et al [14] suggest that progressive depression of excitatory interconnections and activation of Ca^{2+}-dependent K^+ currents eventually terminate neural firing. Compte et al and Bazhenov et al have the same opinion in transitions of neural populations from down to up state. They declare that random summations of miniature EPSPs in some neocortex pyramidal cells are responsible for the switching from down to up state. They assert summations of miniature EPSPs activate persistent Na^+ currents ($I_{Na(p)}$) and generate action potentials. Massimini et al suggest when neurons become hyperpolarized, extra cellular Ca^{2+} concentration is increased linearly and dysfacilitation is removed from the network until neurons resume their firing in up state.

According to Timofeev et al experiments, the slow oscillation is cortical in origin. In a decorticated brain or in a desynchronized cortex, this activity cannot be observed on thalamus and striatum [32, 33], whereas it can be recorded on a deafferented cortex [34]. All aforementioned cortical ionic mechanisms have been introduced as possibly responsible mechanisms for generating the slow oscillation in the brain. However, it should be remembered that other kinds of slow mechanisms may also interfere with ionic mechanisms in the cortex. For example, intrinsic properties of thalamocortical cells ($i.e.$ I_h and I_t ionic currents) generate a stereotype delta oscillations [35]. However it should be noticed that they cannot be reflected at the macroscopic level of the EEG unless thalamic neurons are synchronized by slow oscillations originated from cortical regions [36]. It is also not so clear yet whether EEG delta oscillations are basically come from thalamocortical stereotype oscillations or from waves generated in the cortex.

Instead of engaging with various kinds of slow ionic mechanisms in cortical and subcortical regions, in this paper we propose to formulate their overall characteristics and effects by a generic slow ionic mechanism. This mechanism mainly originates from intrinsic ionic currents of neural cells and it can be represented by a single or coupled slow gating variables. Gating variables should activate/inactivate an inward/outward current in down

state or activate/inactivate an outward/inward current in up state.

It should be emphasized that it is not possible to insert neuronal-level equations of slow gating variables directly in MF models. In fact, gating variables are intrinsic properties of single neurons. For example, an ionic current which is activated in a high voltage by a burst of action potential, would not be activated if it is included in a MF model as it is employed in a single neuron. Their counterparts need to be defined in the context of MF models.

3.3   MODELING SLOW IONIC MECHANISMS IN MF MODELS

We can roughly formulate the activation or inactivation of slow ionic mechanisms or facilitation and dysfacilitation of neurons in a MF model by a slow variable s. Here, we assume that the variable s slowly follows $s_\infty(h_e)$ (an instantly voltage-dependent variable) according to equation (1). $s_\infty(h_e)$ is the activity of the slow mechanism when the membrane potential is kept constant. The slow mechanism is activated in low potentials so $s_\infty(h_e)$ is represented by a descending sigmoid function.

$$\tau_s \frac{d}{dt} s(t) = s_\infty - s(t), \tag{1}$$

$$s_\infty = s_\infty^{\max} / \{1 + \exp(-g_s(h_e - \theta_s))\}, \quad g_s < 0 \tag{2}$$

τ_s is the time constant, $s_\infty^{\max}$ is the maximum value of the sigmoid function, θ_s is the inflection point of the sigmoid function and g_s is the slope at the inflection point.

Equations (1) and (2) show how the membrane potential can influence the activity of the slow mechanism. On the other hand, the slow mechanism is able to modulate the firing rate of neural populations. In the enhanced model, the modulating effect of the slow mechanism is applied on excitatory population. Modulating the excitatory firing rate has indirect effects on other parameters of the model such as excitatory and inhibitory membrane potentials. Increase of s in up or down state increases the firing rate of neural populations. In the down state, an increase of s is equivalent to the removal of dysfacilitation and increase of miniature EPSPs. In the up state, a decrease of s is equivalent to a gradual decrease of firing rate and membrane potential. Equation (3) shows how the excitatory firing rate is modulated by s. In this equation, the previously defined excitatory firing rate in (A4) was renamed $S_e^{prev}(h_e)$.

$$S_e(h_e) = \left[F_1(s) S_e^{prev}(h_e) + F_2(s) S_e^{\mod} \right] \Big/ (F_1(s) + F_2(s)) \tag{3}$$

where,

$$F_1(s) = a(1-B)/\{1+\exp(-g_F(s-\theta_F))\} + b_1 \tag{4}$$

$$F_2(s) = aB/\{1+\exp(g_F(s-\theta_F))\} + b_2 \tag{5}$$

Equation (3) gathers two different terms of firing rates: $S_e^{prev}(h_e)$ and a constant modulating firing rate value S_e^{mod}. The normalized combination of these two terms determines the overall firing rate of the excitatory population. Weighting functions $F_1(s)$ and $F_2(s)$ are anti-symmetric sigmoid functions. B is a free parameter that determines the gain of the modulating term S_e^{mod} by changing the balance between $F_1(s)$ and $F_2(s)$. θ_F and g_F determine the inflection point and slope of the sigmoid functions respectively. g_F is a negative value so $F_1(s)$ and $F_2(s)$ are descending and ascending functions respectively. b_1 and b_2 are two constant values such that set $F_1(0)$ and $F_2(0)$ to one and zero respectively. θ_F determines the convexity of $F_1(s)$ and $F_2(s)$ functions over the interval [0, s_∞^{max}]. Since $F_1(s)$ and $F_2(s)$ are fixed to one and zero respectively at zero, θ_F and g_F may influence the values of these two functions at s_∞^{max}. Parameter a compensates this effect and force $F_1(s)$ and $F_2(s)$ to have the same value at s_∞^{max} for a given B regardless the values of θ_F and g_F. We have chosen $\theta_F = 0.1$, $g_F = -3.5$ as our references for normalization of these functions. If θ_F and g_F be equal to 0.1 and -3.5 respectively, a would be equal to one. In brief, a, b_1 and b_2 are obtained as follows:

$$a = \frac{\left(1+\exp(g_F(s_\infty^{max}-\theta_F))\right)\left(1+\exp(-\theta_F\, g_F)\right)\left(1-\exp(-3.5\, s_\infty^{max})\right)\exp(3.5\times 0.1)}{\left(1+\exp(3.5(0.1-s_\infty^{max}))\right)\left(1+\exp(0.1\times 3.5)\right)\left(1-\exp(g_F\, s_\infty^{max})\right)\exp(-g_F\theta_F)} \tag{6}$$

$$b_1 = 1 - a(1-B)/\{1+\exp(g_F\theta_F)\} \tag{7}$$

$$b_2 = -aB/\{1+\exp(-g_F\theta_F)\} \tag{8}$$

Figure 2 illustrates $F_1(s)$ and $F_2(s)$ for some different values of θ_F and g_F. For each coupled θ_F and g_F values, b_1, b_2 and a are tuned so that boundaries of $F_1(s)$ and $F_2(s)$ do not change for a same given gain of modulating mechanism B.

To study influences of s, θ_F and B on excitatory firing rate, some samples of these variables (*e.g.* {0, 0.33, 0.66, 1}, {0.1, 0.9} and {0.16, 0.04} respectively) are selected and their corresponding excitatory firing rates are sketched in Figure 3. Increasing the s value raises the excitatory firing rate. Activation of the slow mechanism s has more influence on the increase of firing rate in low potentials. This is mainly due to generation of spikes or bursts in low membrane potentials when slow modulating mechanisms are activated. Comparison of left and

right graphs in Figure 3 show that B magnifies the influence of s on firing rate. B does not change excitatory firing rate values corresponding to $s = 0$. By comparing the graphs in top and bottom it can be understood that θ_F may change the ascending patterns of sigmoid functions. However, it does not change the boundary values of the excitatory firing rates. In another word, it does not change excitatory firing rate values corresponding to $s = 0$ and $s = s_\infty^{\max}$ as it was shown in Figure 2.

Figure 2 and Figure 3 around here.

Anesthetic concentration affects amplitudes and decay times of EPSPs and IPSPs as well as the activity of the slow mechanism. For instance, it has been shown that anesthetic drugs in very high concentrations may reduce inward currents [30, 31]. In order to take into account such phenomenon we can reduce the maximum activity of the slow mechanism by reducing B or θ_s values when anesthetic concentration is increased.

4   MODEL SOLUTIONS

A general way to examine the behavior of the variables of the model ($h_k, I_{jk}, \Phi_{ek}, s, \dot{I}_{jk}, \dot{\Phi}_{ek} \big| j, k = \{e, i\}$) is to obtain the numerical solution of the coupled differential equations. If the variables exhibit stable behaviors, generally a good compatibility exists between power spectrums calculated by numerical and analytical methods. Otherwise, when the variables do not converge to equilibrium points, it is not possible to use analytical methods to evaluate their behaviors. Although in such case numerical solution is employed to examine the behavior of the variables, investigations of equilibrium solutions, isoclines and their corresponding vector field may give insights into the behavior of the variables before deriving the numerical solution.

This section is divided into two parts. In the first part, numerical solution of the enhanced model is described. Equilibrium solutions of the model, isoclines and their corresponding vector field are mainly described in the second part.

4.1   NUMERICAL SOLUTION OF THE MODEL

The nine coupled differential equations of the model consist of three first-order and six second-order equations (four of them are stochastic differential equations). Second-order differential equations can be substituted by pairs of first-order differential equations. The general form of the resulted first-order differential equations and their corresponding first-order difference equations are:

$$\frac{d}{dt}x(t) = F(h_e(t), h_i(t)) + A\xi(t),$$ (9)

$$x[n+1] = \left(x[n] + F(h_e[n], h_i[n])\right)\Delta t + A\sqrt{\Delta t}\,\xi[n]$$ (10)

where n is the discrete time, $\xi[n]$ is a zero mean uniform white noise with $\frac{4}{12}$ variance (see (A6)) and Δt is the time increment value (step size) in Euler method, and it was set to 1 ms in our simulations. We could not see any significant changes in numerical results when we used smaller time steps such as 0.1 ms or 0.01 ms.

Basically, the main purpose of performing the numerical simulation of model is to find the time evolution of $h_e(t)$ and $s(t)$ (better to say $h_e[n]$ and $s[n]$) for different anesthetic drug concentrations. In order to do so, drug effects are first applied to IPSP and EPSP parameters (or any other desired parameter such as the slow mechanism) according to equations (A7) and (A8). In the next step, the numerical values of the variables of the model are calculated by Euler one-step scheme for 51.2 seconds. In Euler method, the initial values of the variables are set to their equilibrium values. The simulated signals are down-sampled to 400 Hz in order to be comparable with our real EEG recordings on children [37].

Table 1 lists the numerical values and definitions for the equation parameters and constants. These numerical values are used throughout this paper, except where stated otherwise.

Table 1 around here.

4.2   EQUILIBRIUM SOLUTION, ISOCLINES AND VECTOR FIELD

Equilibrium solution of the model provides much information about the functioning mode of the model. For example, the equilibrium value of $h_e(t)$ may provide some information about the balance between excitatory and inhibitory populations, and the status of the patient such as waking, light or deep anesthesia.

As mentioned before, isoclines may be helpful when the variables of the model do not converge to equilibrium points. To obtain p isoclines in a p-dimensional (pD) hyper-plane, p variables are first selected from the entire m variables of the model, then the equilibrium solution of each variable is calculated while maintaining others to different constant values. The trajectory of the p variables can be sketched in a pD space, but predicting the new position of the trajectory requires obtaining an mD vector field. Directions and lengths of the vectors in this field determine the dynamics of the trajectory. If $p = m$, the vector field can be sketched in the pD space.

By some simplifying assumptions it is possible to reduce the value of m. For example, we can assume that all

10

variables are fast enough compared to h_e, h_i and s to have a simplified model that only consists of three

dynamic variables. Since we are mainly interested to evaluate the role of slow variable s on the EEG signal, we

derive $dh_e/dt = 0$ and $ds/dt = 0$ isoclines (called s,h_e-isoclines) in section 4.2.1. The corresponding vector

field of s,h_e-isoclines is a 3D vector field that cannot be sketched in a plane. In section 4.2.2, we propose a

method that reduces the 3D vector field to a planar vector field. It should be remembered that the 3D simplified

model is only used to obtain the planar vector field. Numerically simulated signals and their corresponding

trajectories (in section 5) are derived from the full model.

4.2.1   ISOCLINES OF THE SLOW MECHANISM AND EXCITATORY MEMBRANE POTENTIAL

One of the best ways to study the influence of slow variable s on the model behavior in different anesthetic

concentration is to sketch s,h_e-isoclines and trajectory of $s(t)$ and $h_e(t)$ signals in a same plane. If ds/dt is

set to zero in (1) and h_e is calculated as a function of s, the result will be $ds/dt = 0$ isocline (simply called

$s-$isocline). On the other hand, declaring s as a function of h_e when $dh_e/dt = 0$ in (A1) results h_e-isocline.

It should be remembered since we only obtain two isoclines of the simplified model, h_i must be set to its

equilibrium value in (A1). In this case, a simple method to calculate h_e-isocline is to vary s between zero and

s_∞^{max} with a definite step size (*e.g.* 0.05) and compute the equilibrium values of h_e and h_i in parallel (they are

referred to as $h_e^\bullet$ and $h_i^\bullet$).

Figure 4 shows two typical superimposed s,h_e-isoclines. Intersections of these two isoclines determine the

equilibrium solutions of the differential equations ($ds/dt = dh_e/dt = 0$). Any other point on the isoclines plane

may have positive or negative values of ds/dt and dh_e/dt . These values can be represented by a vector field.

Length and direction of any given member vector of this vector field show how, s and h_e vary if the state of the

model is located on the origin of that vector.

Figure 4 around here.

4.2.2   OBTAINING PLANAR VECTOR FIELD ON ISOCLINES PLANE

In Figure 4, in addition to s,h_e- isoclines (dashed line and solid line with hexagram marks) we have also shown

nine member vectors of a planar vector field in ($s = 0.4$, $h_e = h_e^\bullet + \Delta h_e$), where $\Delta h_e = \{-1, 0, 1\}$ mV and $h_e^\bullet$'s are red hexagram marks on h_e – isocline. Ordinates and abscissas of the vectors are proportional to ds/dt and dh_e/dt respectively. ds/dt is simply calculated from (1), but obtaining dh_e/dt from (A1) requires more considerations. A glance into equation (A1) reveals that in addition to h_e, h_i also influences the value of dh_e/dt. As a result, since h_i is a dynamic variable in the simplified model, a 3D vector field (dh_e/dt, dh_i/dt, ds/dt) is associated to the model.

To find a planar vector field that can be used instead of the 3D vector field, variable h_i should be replaced by a static value. In order to do so, we examined different planar vectors in different points around h_e – isocline (*i.e.* (s, $h_e^\bullet + \Delta h_e$)). In each given point, planar vectors were different in their abscissas (*i.e.* dh_e/dt) because of the various h_i values that were used in (A1). These values were confined to $h_i^\bullet + \Delta h_i$ values, where $\Delta h_i = \{\pm 1.4, \pm 1.2, ..., \pm 0.2, 0\}$. We observed visually that lengths and directions of vectors for which $\Delta h_i \simeq D/(h_e^\bullet - h_i^\bullet + D)$, $D = 5$ mV, fit well trajectories. As a result, these planar vectors are good candidates to be used instead of 3D vectors. Although these vectors are obtained roughly by this method, it is possible to track simulated signals by a planar vector field (dh_e/dt, ds/dt). This approximation can be used as a useful method for tuning the model parameters and balancing the excitatory and inhibitory factors. It is important to remember that s, h_e – isoclines and their corresponding planar vector field cannot describe the whole dynamics of the model. For example, other variables may start limit cycles that are unpredictable by s, h_e – isoclines; therefore, a numerical solution may still be necessary to confirm results provided by isoclines.

5   BEHAVIOR OF ENHANCED MF MODEL IN VARIOUS DRUG CONCENTRATIONS

In this section, we study the evolution of the EEG signal during various anesthetic concentrations. We perform several numerical simulations in different drug concentrations (from low to high) and describe characteristics and morphologies of the simulated EEG signals. In order to compare the reproduced EEG signals with empirical data, we bring some real EEG signals recorded on children undergoing surgery with Desflurane agent (see [37] to see the protocol of EEG recording). In Desflurane anesthesia, 1 MAC is equivalent to applying 8.3 vol% of this gas to children [38]. This value corresponds to $c \simeq 0.73$ mM aqueous concentrations of Desflurane in saline [39, 40].

Waking and sedation

In the enhanced model, $s, h_e -$ isoclines obtained in waking situation are very similar to those derived for a very low anesthetic drug concentration. Figure 5(a) shows a 10-second (s, h_e) trajectory superimposed on $s, h_e -$ isoclines in $c = 0.2$ mM. Figure 6(a) illustrates that part of the $h_e(t)$ which forms the depicted trajectory in Figure 5(a). The power spectrum of $h_e(t)$ is shown in Figure 7(a) (solid line). In Figure 5(a), coordinates of the intersection point of the two isoclines indicate the equilibrium values of $s(t)$ and $h_e(t)$ signals. The intersection point is located somewhere in the up state area. Head to head directions of the vectors about this equilibrium point indicate that it is a stable equilibrium point. The histogram of $h_e(t)$ in Figure 8(a) also shows that the equilibrium point is stable because h_e fluctuations are centered about a fixed point in the up state area. These fluctuations are actually the result of asynchronous firing mode in neural cells. In such case, the balance between excitatory and inhibitory populations is the most important factor in determining the characteristics of inhibitory and excitatory membrane potentials and firing rates [41]. This balance is mainly determined by (*i*) subcortical noises that are modeled by white uniform noises (p_{jk}), (*ii*) characteristics of IPSPs and EPSPs, (*iii*) connectivity properties of the two populations. In fact, these factors determine a particular model operating state (equilibrium solution) and thus the characteristics of h_e fluctuations. It is straightforward to derive the eigenspectrum (power spectrum) of h_e by taking Fourier transform of the linearized form of the coupled differential equations about their equilibrium values. Figure 7(a) illustrates the analytically calculated eigenspectrum of h_e (dashed line) when drug concentration is 0.2 mM. For comparison, a typical real EEG signal is illustrated in Figure 9(a). This signal is recorded on a child a few seconds before administration of Desflurane agent. The power spectrum of the illustrated EEG signal in Figure 9(a) is shown in Figure 10(a). It should be mentioned that the patient is awake, a little agitated and eyes-open. This situation causes that the energy of alpha band be lower compared with the energy of alpha band in eyes-closed condition.

Figure 5 around here.

Besides focusing on intersections of isoclines and equilibrium solutions of s and h_e, assessing the behavior of the model when s takes different constant values is of interest especially in cases when the trajectory runs away from the attracting area of a stable equilibrium point or when an equilibrium point is unstable. Since h_e converges to its equilibrium value faster than s, on a short time period, s can be assumed constant and the

13

behavior of the trajectory can be mainly thus studied by means of h_e – isocline. It is important to remember that for any point on h_e – isocline, dh_e/dt is equal zero and following the fast convergence of a trajectory to h_e – isocline, dh_e/dt value also converges to zero rapidly. Consequently, in an instability mode, trajectories are mainly located in the vicinity of h_e – isocline, and we generally need to obtain only few members of the planar vector field in the vicinity of h_e – isocline and not over the entire isoclines plane.

In Figure 5(a), h_e – isocline shows that those equilibrium solutions corresponding to $0.25 < s < 1$ make a single branch in the up state area, while those corresponding to $s < 0.25$ make three branches in down, middle and up state areas. Equilibrium points located in the middle branch are unstable. This is known from the opposite directions of planar vectors in the vicinity of these equilibrium points. The probability of finding a trajectory in the vicinity of these points is low. The up state equilibrium points have the highest probability of occurrence compared with the two other types of equilibrium points. If $h_e(t)$ is initialized to a value grater than –64 mV and then it is perturbed by, for example, an inhibitory subcortical activity, there is a high probability that $h_e(t)$ approaches again the up state area. In contrary, vectors about the down state equilibrium points indicate that there are not enough attraction forces toward these points and even if $h_e(t)$ approaches this area, it does not stay for a long time in this state and will switch back again to the up state via a saddle point.

Moderate anesthetic drug concentration (about 1 MAC)

When anesthetic concentration is increased to a higher value (*e.g.* $c = 0.75$ mM) and the balance between excitatory and inhibitory populations shifts a little toward more inhibition, the power spectrum of $h_e(t)$ shifts to lower frequencies. Compared to Figure 5(a), in Figure 5(b) the right branch of h_e – isocline has moved a little to more negative potentials and the inverse U-turn has moved to up and right sides. Since s positively modulates the excitatory firing rate in equation (3), movement of the inverse U-turn toward more positive s values indicates that the balance has moved to inhibition. As a result, for example when s is equal to 0.4 mM three equilibrium points exist on h_e – isocline depicted on Figure 5(b), while for the same s value, only one equilibrium point can be found on h_e – isocline reported on Figure 5(a). When the distance between right and middle branches of h_e – isocline is reduced, $h_e(t)$ is distributed over a wider region along the up state area so the probability of the trajectory for being in the neighborhood of the middle branch is increased. This can cause the trajectory to move along or cross the barrier of the unstable branch to reach the down state area. This is the beginning phase of slow wave episodes on EEG signal. At first, most of trajectory cycles encounter the attraction

of the up state area and the repulsion of the middle branch so they move back to the up state area. Those who reach the down state area appear semi-periodic high amplitude negative pulses on $h_e(t)$ illustrated in Figure 6(b). Appearance of such negative pulses extends the histogram of the h_e signal toward negative potentials (see Figure 8(b)), but since most of the time h_e activities are related to the up state, the histogram still contains a single peak located in the up state area. Negative pulses of $h_e(t)$ increase the overall power especially in the slow delta band (0-2 Hz). Figure 7(b) illustrates a typical power spectrum of $h_e(t)$ when drug concentration is 0.75 mM.

Figure 6 - Figure 7 - Figure 8 around here.

Figure 9(b) shows a typical real EEG signal recorded at 1 MAC Desflurane. A combination of high amplitude, low frequency negative peaks and low amplitude, high frequency activities is seen on the real EEG signal like what can be observed on simulated signal in Figure 6(b). However, it should be mentioned that amplitudes of negative slow waves on real signals may vary accidentally in successive EEG epochs. This variation may increase the standard deviation of EEG energy. It seems that interactions of different modulating mechanisms and their overall effects on the brain activity and so synchronization of neural cells in a local field may be influenced by past non-full-periodic activities of slow negative pulses. However, this is a subject that we do not deal with in this study.

Increasing the anesthetic concentration a bit more (*e.g.* c = 0.9 mM), makes it possible for trajectories to jump over the barrier of the unstable area and change the state of the model from up to down easier than before. Figure 5(c) shows 10 seconds of (s, h_e) trajectory when c is equal 0.9 mM (see also Figure 6(c), Figure 7(c) and Figure 8(c) that show the time course, power spectrum and histogram of $h_e(t)$ respectively). In transition from up to down state, the value of s increases gradually following the rapid change of s_∞ value. Increase of s continues until the trajectory approaches a saddle point (tip of the inverse U-turn). This point is the critical point where sufficient modulating factors have been accumulated in the excitatory neural population; therefore the trajectory switches back to the up state. When the switching is taken place, s is then gradually decreased until another transition from up to down state happens.

As illustrated in Figure 6(c), the transition rate between the two states has increased compared to the case where c =0.75 mM. The histogram of $h_e(t)$ has now two distinct peaks that are related to down and up states

15

respectively (Figure 8(c)). But as it is shown in Figure 5(c), the trajectory is still mainly located in the up state area and as a consequence, the amplitude of the second peak of the histogram is higher than the first one.

Figure 9 and Figure 10 around here.

Figure 9(c) illustrates a real EEG signal recorded in a drug concentration that is a bit higher than 1 MAC [37]. It should be mentioned that Compared to Figure 9(b), the number of negative peaks is increased and the EEG background activity is replaced by a lower frequency higher amplitude activity.

High anesthetic drug concentration (about 2 MAC)

We have determined the equilibrium solution of h_e and studied their linear stability when anesthetic drug concentration is varied between 0 and 1.8 mM. Figure 11 displays the results where stars and circles correspond to stable and unstable solutions respectively. For a wide range of anesthetic drug concentration, simulated EEG signals have almost the same morphologies. Therefore, we select a candidate concentration value within this range to examine the behavior of the model. Figure 5(d) represents $s, h_e -$ isoclines corresponding to $c = 1.5$ mM. The intersection of the two isoclines occurs in the middle branch of $h_e -$ isocline. Linear stability analysis shows that the model has a unique equilibrium point which is unstable.

Figure 11 around here.

The time course and power spectrum of the numerically simulated h_e signal in Figure 6(d) and Figure 7(d) show that the rate of negative peaks in $h_e(t)$ is more or less similar to what we had for $c = 0.9$ mM and it is higher than what we had for $c = 0.75$ mM. Figure 6(d) also shows that the switching between up and down states is more regular. This can also be testified by means of the histogram of h_e fluctuations which depicts two dominant peaks.

Figure 9(d) illustrates a real EEG signal at 2 MAC [37]. Visually inspection of this figure shows that our model is still able to generate signals miming real EEG recordings. The power spectrum of the EEG signal, basically, consists of a semi-periodic 2.3 Hz activity. Due to this semi-periodic activity, the power of fast delta band (*e.g.* 2-4 Hz) may even become greater than the power of slow delta band (*e.g.* 0-2 Hz) at 2 MAC [42]. Similar behavior is expressed by simulated data (see Figure 7(d)).

Burst-Suppression

EEG suppression is the last phenomenon to be observed in very deep anesthesia. About 30 percent of EEG signals in Tirel *et al* experiment [37], exhibit suppressed activity at 2 MAC Desflurane anesthesia. Sometimes EEG suppressions alternate with bursting activities. This phenomenon is the so-called burst-suppression pattern. Bursts result from short-time discharges of single cells action potentials. Although the enhanced model was not optimized for simulating burst-suppression patterns, it is able to qualitatively reproduce EEG dynamics showing bursting activities and the transition toward full suppression.

A burst is generated when neural cells jump temporarily from down to up state. The enhanced model can reproduce such activity if $s, h_e -$ isoclines intersect in the down state area in the vicinity of the unstable middle branch of $h_e -$ isocline. For example, if we keep all parameters of the model constant but reduce the modulation strength of the slow mechanism slightly (*e.g.* $B = 0.14$, $\theta_s = -60$), burst-suppression is generated. Figure 12 shows the two isoclines of the model when drug concentration is 1.8 mM. The intersection of the two isoclines is very close to the saddle point of the $h_e -$ isocline so (s, h_e) trajectory that is generally located in the vicinity of the down state equilibrium point, may sometimes switch to the up state for short periods. Figure 13 shows $h_e(t)$ corresponding to the illustrated trajectory in Figure 12. The histogram of h_e which only consists of a single peak in the down state area is depicted in Figure 14.

By decreasing the drug concentration, $h_e -$ isocline moves toward negative direction of $s -$ axis so the equilibrium point becomes closer to the middle branch of $h_e -$ isocline (unstable area). Consequently, (s, h_e) trajectory may escape from the down state area easier than before. This increases the number of bursts on the EEG signal which is in agreement with Bruhn's experiments [43, 44]. On the other hand, increasing the drug concentration or blocking the slow modulating mechanisms reduces the possibility of burst generation. In such case the model may remain in suppressed mode if subcortical inputs do not activate the model by triggering events.

Figure 12, Figure 13 and Figure 14 around here.

6   DISCUSSIONS AND CONCLUSIONS

Modeling is unavoidably based on simplifications of real systems. In our viewpoint, the simpler the model that

can explain a particular phenomenon, the more fundamental is its scope. The proposed MF model encompasses the two most important neural populations in the neocortex (pyramidal and interneurons) and a slow mechanism that modulates the firing rate of pyramidal population. It is an easy to understand model by which we can study the role of inhibitory and excitatory factors as well as the slow modulating mechanism of excitatory firing rate in various anesthetic concentrations.

Since internal states of a neural network and single neurons are closely related to each other, a population of neural cells may exhibit bursts of activities (like single neurons) even if it has been settled in down state. Without including any modulating parameter in the model, a static form of the sigmoid relationship between the mean membrane potential and firing rate does not justify the generation of bursts in very low potentials. We redefined the sigmoid relationship and included the influence of a typical slow modulating mechanism. Out of various types of modulating parameters that may modulate the mean firing rate of a neural population, we only considered a generic slow voltage-dependent ionic current. It should be remembered that there are many kinds of modulating mechanisms in the brain and each mechanism may have its own characteristics (*e.g.* different time constants) and may exhibit different behaviors in different anesthetic drug concentrations. In this model, the overall effects of all types of slow mechanisms have been gathered in a voltage-dependent mechanism leading to a new functioning mode (*i.e.* up and down states) which better explain the occurrence of high amplitude slow waves in EEG. However, in order to further improve the model, MF characteristics of the most important modulating mechanisms in cortical and subcortical areas should be identified and incorporated.

Compared to previous MF models, the working modes of the enhanced model are closer to some neurophysiological observations. For example, experimental results show that in an overall view, neural cells activities may be classified to continuous, phasic or silence. The single point equilibrium solution of the model in each drug concentration (Figure 11) is in accordance with this classification. If this single point equilibrium solution is stable, it represents either a high firing-rate continuous activity (up state) or silence (down state). If the equilibrium solution is unstable or very close to unstable region, it corresponds to switching of neural activities between the two states.

Nonsmoothly variation of stable equilibrium solutions [7, 8] is not in agreement with a smooth reduction of neural firing rates with anesthetic drug concentration [26]. A single stable branch in various drug concentrations [9] does not justify the two different firing states of neural populations (*e.g.* in slow waves or burst-suppression). On the contrary, equilibrium solutions of the enhanced model vary smoothly in a dose-dependant manner from up to down state. This model considers the two firing states of neural populations so it can reproduce some

internal states of neural populations [23] such as continuous activities in up state, transient jumps from up to down state, regular switching between up and down states, burst-suppression and suppression. In general, the maximum firing rate value of a neural population does not change noticeably before and after applying an anesthetic agent [26]. The mean firing rate value of a neural population is mainly reduced by the occurrence of silence phase between firing phases [16]. Firing patterns of neural populations of the enhanced model (see Figure 15) are in agreement with these remarks, while in previous MF models, mean and maximum firing rates values are jointly reduced by increasing anesthetic concentration.

Figure 15 around here.

In the enhanced model, the sudden transition between awareness and unconsciousness may be interpreted by sudden transition between internal states of neural populations induced by similar behaviors in single neurons [23]. According to different activity modes represented in section 5, it is probable that awareness-unconsciousness are two disjoint mental states because firing patterns of neural populations are changed suddenly from continuous mode to phasic mode as if the information processing mode of the brain is changed suddenly by administrating an anesthetic agent. Such a result needs to be confirmed by experimental data showing the evolution of neural membrane potentials and firing rates during awareness-unconsciousness transition.

 The enhanced model has also some limitations. A single homogeneous neocortical module is introduced without considering other parts of brain such as thalamus and hippocampus; therefore, it is not forced to reproduce some typical EEG activities such as spindles and alpha rhythm that are generated in these parts of the brain. It has been suggested that spindles are generated in the thalamus [45] and corticothalamic inputs control the patterns of activities in thalamus and thalamocortical networks [46, 47]. Recent studies show that a distributed alpha network which consists of thalamus, cortex and hippocampus is engaged in alpha oscillations. A communication exists between neocortex and hippocampus during alpha oscillations [48] and hippocampus can react to sensory stimuli with a 10 Hz enhancement [49].

In future studies, a model aimed at generating slow and delta rhythms as well as spindles and alpha rhythm will be built by integrating underlying synaptic and ionic mechanisms located in cortical and subcortical regions. It would be useful also to expand the enhanced model to a nonhomogenous one.

It should be emphasized that in a stable situation, the amplitude of simulated EEG signal (h_e) is mainly

determined by variance of input noises and characteristics of the transfer function of the model, but in an unstable situation (limit-cycle), it is mainly determined by the potential difference between left and right branches of h_e – isocline (*i.e.* up and down states). However, because of individual dissimilarities in the structures of different single neural cells, they may switch to up and down state not in a fully synchronized manner. According to our EEG recordings on children (Figure 9) and Constant *et al* experiments [50] it can be inferred that the amplitude ratio is almost equal to 10 before and after administration of anesthetics. The amplitude ratio of reproduced EEG signals (Figure 6) is comparable with the empirical amplitude ratio in children, but it is higher than the amplitude ratio in adults [51]. It has been stated that this amplitude ratio is decreased by age and maturation of neural cells [50, 51]. Such increase in amplitude ratio is also observed in reproduced K-complexes in Wilson *et al* model [52]. The amplitude ratio of K-complexes to background EEG activities in this model is slightly higher than the one in empirical data [19]. It seems that maturation of neural cells or equivalently specialization of neural cells to do more specific tasks in the brain induces less similarity between them. As a result, synchronization between adjacent neural cells in a local field is higher for children than for adults.

One of the basic assumptions in designing population equations is that neural cells are identical and have similar properties in a volume of one macrocolumn. Prominent examples are columns in the somatosensory and visual cortex and pools of motor neurons. Dissimilarities in structure and function of neural cells in a local field degrade the above assumption; so it seems that maturation of neural cells and their potency of synchronization are still required to be considered somehow (for example, by dividing inhibitory and excitatory populations into some subpopulations and randomizing their parameters) in MF models. This may fill the gap which exists between full-synchronous and asynchronous activities.

At last, we want to mention that *biphasic* is a transient dynamic response of the brain which is basically originated from fast variations of brain inputs (e.g. drug concentration) during the time. It is shown that changing the speed of the administration of an anesthetic drug changes the characteristics of biphasic response and the concentration in which the maximum of the biphasic response appears [15]. In general, at a given drug concentration, EEG amplitudes are not identical in steady-state and transient conditions. Behavior of our enhanced MF model is discussed in steady-state condition so a simulated EEG signal in this condition should be compared with a real EEG signal recorded in steady-state condition not in transient condition.

APPENDIX I

This appendix briefly describes the basic equations of the enhanced MF model that were derived from the pioneering works of Steyn-Ross *et al* [6-8] and Bojak & Liley [9]. Since these equations are now well-covered in many other journals, we do not define them in so much detail. For definitions of the parameters of the model see table 1.

Equation (A1) depicts the two main differential equations of the model that express mean membrane potentials of inhibitory and excitatory populations (h_e, h_i).

$$\tau_k \frac{dh_k(t)}{dt} = h_k^{rest} - h_k + \psi_{ek}(h_k)I_{ek}(h_e) + \psi_{ik}(h_k)I_{ik}(h_i) \quad k = \{e, i\} \tag{A1}$$

$$\psi_{jk}(h_k) = \left[h_j^{rev} - h_k \right] \Big/ \left| h_j^{rev} - h_k^{rest} \right| \tag{A2}$$

j and k may represent either excitatory (e) or inhibitory (i). ψ_{jk} is a scaling factor and indicates the potency of synapses between j and k-type populations. I_{jk} represents voltaic influences of synapses and is represented in (A3) by convolving the firing rate of k population and j-type post synaptic potential (PSP) function. The bracketed term in right hand side of (A3) represents the firing rate of k-type population which is composed of three sources: locally in the same macrocolumn (S_j), distant from other macrocolumns (Φ_{jk}) and subcortical inputs (p_{jk}).

$$\left(\frac{d}{dt} + \gamma_j \right) \left(\frac{d}{dt} + \tilde{\gamma}_j \right) I_{jk}(t) = [N_{jk}^\beta S_j(h_j) + \Phi_{jk} + p_{jk}]G_j\tilde{\gamma}_j e^{\gamma_j \delta_j(\gamma_j, \tilde{\gamma}_j)} \quad j, k = \{e, i\} \tag{A3}$$

PSPs are represented by biexponential functions. G_j, γ_j and $\tilde{\gamma}_j$ determine maximum values, rising and falling time constants of the biexponential functions. These parameters are varied by anesthetic drug concentrations. Instead of directly applying the influence of anesthetic drugs on γ_j and $\tilde{\gamma}_j$, it is more convenient to define two alternative parameters (δ_j and ζ_j) and then modify them by drug concentration [9]. δ_j is the time lag of PSP maximum peak and ζ_j is the decay time of PSP function.

S_j determines the mean firing rate of j-type population from mean membrane potential. A sigmoid function is

employed to represent this relationship [53].

$$S_j(h_j) = S_j^{\max} / \{1 + \exp[-g_j(h_j - \theta_j)]\} \tag{A4}$$

where $S_j^{\max}$ denotes the maximum firing rate; θ_j and g_j respectively determine the inflection point and its slope in the sigmoid function.

Distant generated firing rates (Φ_{jk}) are only confined to excitatory originated because the long-distance coupling from inhibitory populations is unlikely ($\Phi_{ik} = 0$). Φ_{ek} is determined by applying a spatial-temporal filter on $S_e(h_e)$. Since the brain has been assumed to be a homogeneous media no spatial variable is seen in (A5).

$$\left(\frac{d}{dt} + \overline{v}\Lambda_{ek}\right)^2 \Phi_{ek}(t) = \overline{v}^2 \Lambda_{ek}^2 N_{ek}^\alpha S_e(h_e) \tag{A5}$$

For simplicity, each subcortical noise is modeled by equation (A6). However, it should be mentioned that there are also other formulations for representations of subcortical noises [9, 54] that may be employed in more specialized studies according to their specific purposes. In equation (A6), $\overline{p}_{jk}$ is a constant value and represents the incoming mean firing rate of the j-type subcortical population to k-type cortical population. $\xi_{jk}(t)$ is a zero mean uniform white noise that extends between -1 and +1, so the variance of $\overline{p}_{jk}$ is equal to $\alpha^2 \overline{p}_{jk}^2 / 3$. α is a scaling factor that controls the variance of the noises and can be used to prevent the generation of negative value noises in numerical simulations.

$$p_{jk}(t) = \overline{p}_{jk} + \alpha \overline{p}_{jk} \xi_{jk}(t) \tag{A6}$$

Administration of anesthetic drugs changes the shape of PSPs. Based on real experimental data it is possible to relate amplitude and time constant of IPSP or EPSP to different anesthetic drug concentration. We used the following Hill equations (for more discussion see Ref. [9, 55]) to express variations of maximum amplitudes and decay times of IPSPs and EPSPs in different concentration of a generic anesthetic drug:

$$G_j(c_{MAC}) = G_j^0 \frac{K_j^{N_j} + M_j c_{MAC}^{N_j}}{K_j^{N_j} + c_{MAC}^{N_j}} \qquad j = \{i, e\} \tag{A7}$$

$$\zeta_i(c_{MAC}) = \zeta_i^0 \frac{k_i^{n_i} + m_i c_{MAC}^{n_i}}{k_i^{n_i} + c_{MAC}^{n_i}}, \qquad \zeta_e(c_{MAC}) = \zeta_e^0 \tag{A8}$$

where c_{MAC} is the alveolar drug concentration in MAC (1 MAC is the minimum alveolar concentration of an anesthetic agent at 1 atmosphere pressure at which 50% of patients still move in response to a noxious stimulus).

22

K_i, M_i, N_i, K_e, M_e, N_e, k_i, m_i and n_i are free parameters of Hill equations that have been assigned with 1.25, 0.37, 2.3, 2.5, 0.5, 1, 0.975, 4.4 and 2.8 respectively for our generic anesthetic drug. G_j^0 and ζ_j^0 are maximum amplitude and decay time of j–type PSP at zero drug concentration.

In this paper we use 1 MAC = 8.3 vol% for Desflurane. This is appropriate for young children [38] and corresponds to $c_{Aq} \simeq 0.73$ mM aqueous concentration of Desflurane in saline [39, 40] considering that saline/gas partition coefficient is equal 0.225 for Desflurane [56].

To express equations (A7) and (A8) as functions of aqueous concentration of Desflurane (c_{Aq}) or vol% (c_{vol}), it is only necessary to replace K_j and k_i with μK_j and μk_i where μ is equal to 0.73 and 8.3 for c_{Aq} and c_{vol} respectively. In this study, we express the concentration of Desflurane (c) by its aqueous concentration c_{Aq}.

REFERENCES

[1]   L. Senhadji, E. Wodey, and E. Claude, "Monitoring approaches in general anesthesia: a survey," *Crit. Rev. Biomed. Eng.*, vol. 30, pp. 85-97, 2002.

[2]   W. Gerstner and W. M. Kistler, *Spiking Neuron Models : Single Neurons, Populations, Plasticity*: Cambridge University Press, 2002.

[3]   A. Renart, N. Brunel, and X. J. Wang, "Mean-Field Theory of Irregularly Spiking Neuronal Populations and Working Memory in Recurrent Cortical Networks," in *Computational Neuroscience: A Comprehensive Approach, Chapman & Hall/CRC Mathematical Biology and Medicine Series*, J. Feng, Ed. Boca Raton: CRC Press, 2003, pp. 431-490.

[4]   D. T. J. Liley, P. J. Cadusch, and J. J. Wright, "A continuum theory of electro-cortical activity," *Neurocomputing*, vol. 26-27, pp. 795-800, 1999.

[5]   D. T. Liley, P. J. Cadusch, and M. P. Dafilis, "A spatially continuous mean field theory of electrocortical activity," *Network*, vol. 13, pp. 67-113, 2002.

[6]   M. L. Steyn-Ross, D. A. Steyn-Ross, and J. W. Sleigh, "Modelling general anaesthesia as a first-order phase transition in the cortex," *Prog Biophys Mol Biol*, vol. 85, pp. 369-85, 2004.

[7]   M. L. Steyn-Ross, D. A. Steyn-Ross, J. W. Sleigh, and L. C. Wilcocks, "Toward a theory of the general-anesthetic-induced phase transition of the cerebral cortex. I. A thermodynamics analogy," *Phys Rev E Stat Nonlin Soft Matter Phys*, vol. 64, pp. 011917, 2001.

[8]   D. A. Steyn-Ross, M. L. Steyn-Ross, L. C. Wilcocks, and J. W. Sleigh, "Toward a theory of the general-anesthetic-induced phase transition of the cerebral cortex. II. Numerical simulations, spectral entropy, and correlation times," *Phys Rev E Stat Nonlin Soft Matter Phys*, vol. 64, pp. 011918, 2001.

[9]   I. Bojak and D. T. Liley, "Modeling the effects of anesthesia on the electroencephalogram," *Phys Rev E Stat Nonlin Soft Matter Phys*, vol. 71, pp. 041902, 2005.

[10]   T. G. Weyand, M. Boudreaux, and W. Guido, "Burst and Tonic Response Modes in Thalamic Neurons During Sleep and Wakefulness," *J Neurophysiol*, vol. 85, pp. 1107-1118, 2001.

[11]   M. Steriade, I. Timofeev, and F. Grenier, "Natural Waking and Sleep States: A View From Inside Neocortical Neurons," *J Neurophysiol*, vol. 85, pp. 1969-1985, 2001.

[12]   A. Compte, M. V. Sanchez-Vives, D. A. McCormick, and X. J. Wang, "Cellular and network mechanisms of slow oscillatory activity (<1 Hz) and wave propagations in a cortical network model," *J Neurophysiol*, vol. 89, pp. 2707-25, 2003.

[13]   M. Massimini and F. Amzica, "Extracellular calcium fluctuations and intracellular potentials in the cortex during the slow sleep oscillation," *J Neurophysiol*, vol. 85, pp. 1346-50, 2001.

[14]   M. Bazhenov, I. Timofeev, M. Steriade, and T. J. Sejnowski, "Model of thalamocortical slow-wave sleep oscillations and transitions to activated States," *J Neurosci*, vol. 22, pp. 8691-704, 2002.

[15]   K. Kuizenga, J. H. Proost, J. M. Wierda, and C. J. Kalkman, "Predictability of processed electroencephalography effects on the basis of pharmacokinetic-pharmacodynamic modeling during repeated propofol infusions in patients with extradural analgesia," *Anesthesiology*, vol. 95, pp. 607-15, 2001.

[16]   B. Antkowiak and D. Heck, "Effects of the volatile anesthetic enflurane on spontaneous discharge rate and GABA(A)-mediated inhibition of Purkinje cells in rat cerebellar slices," *J Neurophysiol*, vol. 77, pp. 2525-38, 1997.

[17]   B. Antkowiak and C. Helfrich-Forster, "Effects of small concentrations of volatile anesthetics on action potential firing of neocortical neurons in vitro," *Anesthesiology*, vol. 88, pp. 1592-605, 1998.

[18]   D. Pare, E. Shink, H. Gaudreau, A. Destexhe, and E. J. Lang, "Impact of spontaneous synaptic activity on the resting properties of cat neocortical pyramidal neurons In vivo," *J Neurophysiol*, vol. 79, pp. 1450-60, 1998.

[19]   F. Amzica and M. Steriade, "The functional significance of K-complexes," *Sleep Medicine Reviews*, vol. 6, pp. 139-149, 2002.

[20]   C. Bedard, H. Kroger, and A. Destexhe, "Modeling extracellular field potentials and the frequency-filtering properties of extracellular space," *Biophys J*, vol. 86, pp. 1829-42, 2004.

[21]   M. Rudolph, J. G. Pelletier, D. Pare, and A. Destexhe, "Characterization of synaptic conductances and integrative properties during electrically induced EEG-activated states in neocortical neurons in vivo," *J Neurophysiol*, vol. 94, pp. 2805-21, 2005.

[22]   A. Destexhe, M. Rudolph, J. M. Fellous, and T. J. Sejnowski, "Fluctuating synaptic conductances recreate in vivo-like activity in neocortical neurons," *Neuroscience*, vol. 107, pp. 13-24, 2001.

[23]   S. Fujisawa, N. Matsuki, and Y. Ikegaya, "Single Neurons Can Induce Phase Transitions of Cortical Recurrent Networks with Multiple Internal States," *Cereb Cortex*, 2005.

[24]   B. Antkowiak, H. Hentschke, and K. Kirschfeld, "Effects of volatile anaesthetics on spontaneous action potential firing of cerebellar Purkinje cells in vitro do not follow the Meyer-Overton rule," *Br. J. Anaesth.*, vol. 79, pp. 617-624, 1997.

[25]   K. Nishikawa and M. B. MacIver, "Agent-selective effects of volatile anesthetics on GABAA receptor-mediated synaptic inhibition in hippocampal interneurons," *Anesthesiology*, vol. 94, pp. 340-7, 2001.

[26]   B. Antkowiak, "Different actions of general anesthetics on the firing patterns of neocortical neurons mediated by the GABA(A) receptor," *Anesthesiology*, vol. 91, pp. 500-11, 1999.

[27]   B. Antkowiak, "How do general anaesthetics work?," *Naturwissenschaften*, vol. 88, pp. 201-13, 2001.

[28]   P. G. Barash, B. F. Cullen, and R. K. Stoetting, "Cellular and Molecular Mechanisms of Anesthesia," in *Clinical Anesthesia*, Fifth ed, 2005, pp. 111-131.

[29]   D. Bleakman, M. V. Jones, and N. L. Harrison, "The effects of four general anesthetics on intracellular [Ca2+] in cultured rat hippocampal neurons," *Neuropharmacology*, vol. 34, pp. 541-51, 1995.

[30]   C. R. Ries and E. Puil, "Ionic mechanism of isoflurane's actions on thalamocortical neurons," *J Neurophysiol*, vol. 81, pp. 1802-9, 1999.

[31]   C. R. Ries and E. Puil, "Mechanism of anesthesia revealed by shunting actions of isoflurane on thalamocortical neurons," *J Neurophysiol*, vol. 81, pp. 1795-801, 1999.

[32]   I. Timofeev and M. Steriade, "Low-frequency rhythms in the thalamus of intact-cortex and decorticated cats," *J Neurophysiol*, vol. 76, pp. 4152-68, 1996.

[33]   F. Kasanetz, L. A. Riquelme, and M. G. Murer, "Disruption of the two-state membrane potential of striatal neurones during cortical desynchronisation in anaesthetised rats," *J Physiol*, vol. 543, pp. 577-89, 2002.

[34]   I. Timofeev, F. Grenier, M. Bazhenov, T. J. Sejnowski, and M. Steriade, "Origin of Slow Cortical Oscillations in Deafferented Cortical Slabs," *Cereb. Cortex*, vol. 10, pp. 1185-1199, 2000.

[35]   M. Steriade, A. Nunez, and F. Amzica, "Intracellular analysis of relations between the slow (< 1 Hz) neocortical oscillation and other sleep rhythms of the electroencephalogram," *J. Neurosci.*, vol. 13, pp. 3266-3283, 1993.

[36]   M. Steriade, R. C. Dossi, and A. Nunez, "Network modulation of a slow intrinsic oscillation of cat thalamocortical neurons implicated in sleep delta waves: cortically induced synchronization and brainstem cholinergic suppression," *J Neurosci*, vol. 11, pp. 3200-17, 1991.

[37]   O. Tirel, E. Wodey, R. Harris, J. Y. Bansard, C. Ecoffey, and L. Senhadji, "The impact of age on bispectral index values and EEG bispectrum during anaesthesia with desflurane and halothane in children," *Br J Anaesth*, vol. 96, pp. 480-5, 2006.

[38]   W. W. Mapleson, "Effect of age on MAC in humans: a meta-analysis," *Br J Anaesth*, vol. 76, pp. 179-85, 1996.

[39]   N. P. Franks and W. R. Lieb, "Selective actions of volatile general anaesthetics at molecular and cellular levels," *Br J Anaesth*, vol. 71, pp. 65-76, 1993.

[40]   N. P. Franks and W. R. Lieb, "Temperature dependence of the potency of volatile general anesthetics: implications for in vitro experiments," *Anesthesiology*, vol. 84, pp. 716-20, 1996.

[41]   N. Brunel and X.-J. Wang, "What Determines the Frequency of Fast Network Oscillations With Irregular Neural Discharges? I. Synaptic Dynamics and Excitation-Inhibition Balance," *J Neurophysiol*, vol. 90, pp. 415-430, 2003.

[42]   B. Molaee Ardekani, M. B. Shamsollahi, L. Senhadji, E. Wodey, and B. Vosoughi Vahdat, "An Investigation on Different EEG Patterns From Awake to Deep Anesthesia: Application to improve methods of determining depth of anesthesia," presented at World Congress on Medical Physics and Biomedical Engineering WC2006, Seoul-Korea, 2006.

[43]   J. Bruhn, H. Ropcke, B. Rehberg, T. Bouillon, and A. Hoeft, "Electroencephalogram Approximate Entropy Correctly Classifies the Occurrence of Burst Suppression Pattern as Increasing Anesthetic Drug Effect," *Anesthesiology*, vol. 93, pp. 981-5, 2000.

[44]   J. Bruhn, T. W. Bouillon, and S. L. Shafer, "Bispectral index (BIS) and burst suppression: revealing a part of the BIS algorithm," *J Clin Monit Comput*, vol. 16, pp. 593-6, 2000.

[45]   M. Steriade, L. Domich, G. Oakson, and M. Deschenes, "The deafferented reticular thalamic nucleus generates spindle rhythmicity," *J Neurophysiol*, vol. 57, pp. 260-73, 1987.

[46]   H. Blumenfeld and D. A. McCormick, "Corticothalamic inputs control the pattern of activity generated in thalamocortical networks," *J Neurosci*, vol. 20, pp. 5153-62, 2000.

[47]   A. Destexhe, D. Contreras, and M. Steriade, "Cortically-induced coherence of a thalamic-generated oscillation," *Neuroscience*, vol. 92, pp. 427-43, 1999.

[48]   A. Sirota, J. Csicsvari, D. Buhl, and G. Buzsaki, "Communication between neocortex and hippocampus during sleep in rodents," *PNAS*, vol. 100, pp. 2065-2069, 2003.

[49]   M. Schurmann, T. Demiralp, E. Basar, and C. Basar Eroglu, "Electroencephalogram alpha (8-15 Hz) responses to visual stimuli in cat cortex, thalamus, and hippocampus: a distributed alpha network?," *Neurosci Lett*, vol. 292, pp. 175-8, 2000.

[50]   I. Constant, R. Seeman, and I. Murat, "Sevoflurane and epileptiform EEG changes," *Paediatr Anaesth*, vol. 15, pp. 266-74, 2005.

[51]   A. Schultz, U. Grouven, I. Zander, F. A. Beger, M. Siedenberg, and B. Schultz, "Age-related effects in the EEG during propofol anaesthesia," *Acta Anaesthesiol Scand*, vol. 48, pp. 27-34, 2004.

[52]   M. T. Wilson, D. A. Steyn-Ross, J. W. Sleigh, M. L. Steyn-Ross, L. C. Wilcocks, and I. P. Gillies, "The K-complex and slow oscillation in terms of a mean-field cortical model," *J Comput Neurosci*, vol. 21, pp. 243-57, 2006.

[53]   H. R. Wilson and J. D. Cowan, "Excitatory and inhibitory interactions in localized populations of model neurons," *Biophys J*, vol. 12, pp. 1-24, 1972.

[54]   G. D. Smith, C. L. Cox, S. M. Sherman, and J. Rinzel, "A firing-rate model of spike-frequency adaptation in sinusoidally-driven thalamocortical relay neurons," *Thalamus and Related Systems*, vol. 1, pp. 135-156, 2001.

[55]   D. T. Liley and I. Bojak, "Understanding the transition to seizure by modeling the epileptiform activity of general anesthetic agents," *J Clin Neurophysiol*, vol. 22, pp. 300-13, 2005.

[56]   E. I. Eger, 2nd, "Partition coefficients of I-653 in human blood, saline, and olive oil," *Anesth Analg*, vol. 66, pp. 971-3, 1987.
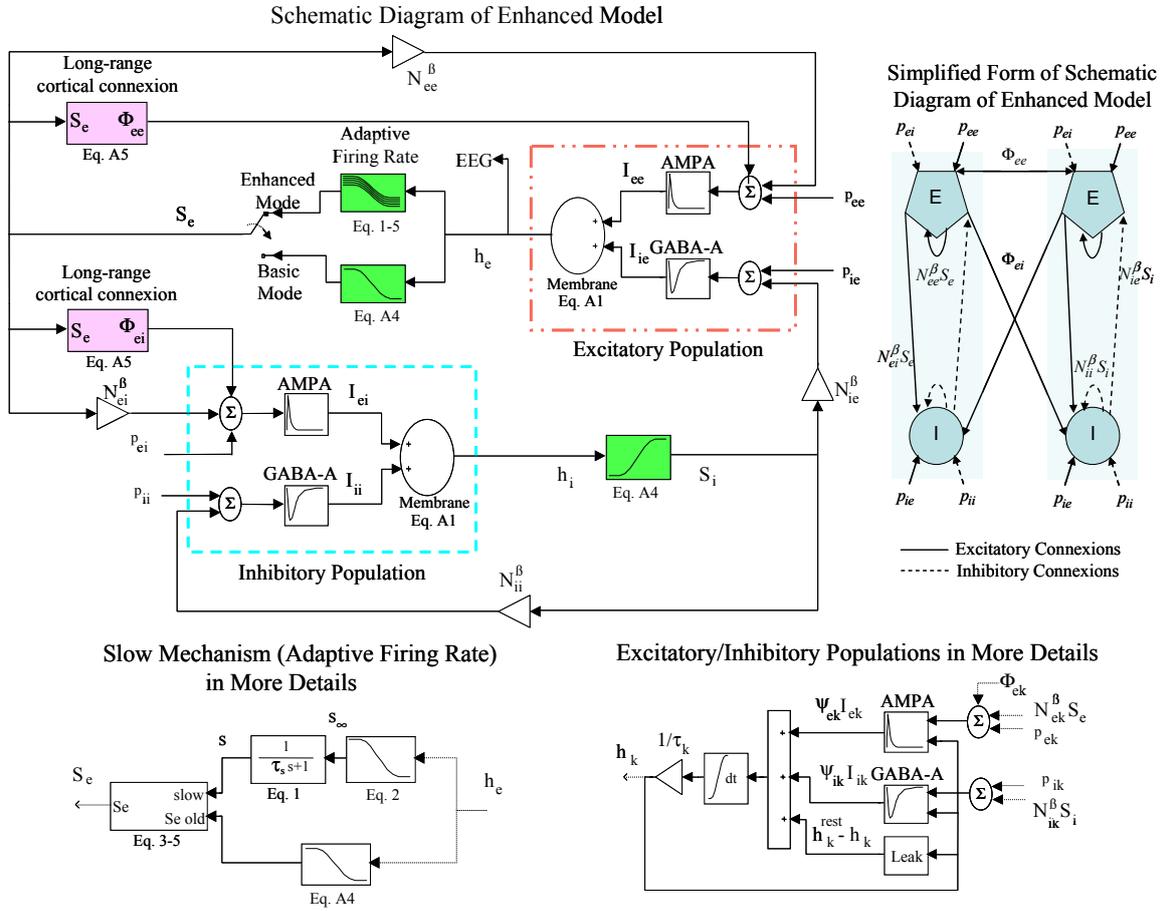
(Color online) Figure 1 : Schematic diagram of the enhanced model. The enhanced model considers the brain as a homogenous media without any kind of specialized subcortical areas. Subcortical activities are modeled by four white noises (p_{jk} | $j,k \in \{e,i\}$) that drive the excitatory (pyramidal) and inhibitory (inter-neurons) populations in the neocortex. Mean membrane potential of each population (h_k) is determined by inhibitory and excitatory post synaptic potentials (I_{jk}) generated by GABA$_A$ and AMPA receptors. The model in its basic mode (see Appendix I) incorporates two sigmoid functions for determining mean firing rates of populations (S_k) from their mean membrane potentials. In addition to short-range influences of neural firing rates on GABA$_A$ and AMPA receptors, excitatory firing rate has also long-rage influences on pyramidal and inter-neurons by the means of AMPA receptor. In the enhanced mode, the static sigmoid function corresponding to the excitatory population is substituted by a slow dynamic equation. A more detailed block diagram related to the slow dynamic equation (see section 3.3) and excitatory/inhibitory populations (see appendix I) have been illustrated in the bottom of the figure.

(a) $g_F = -3.5, \quad B = 0.16$

(b) $g_F = -7, \quad B = 0.16$
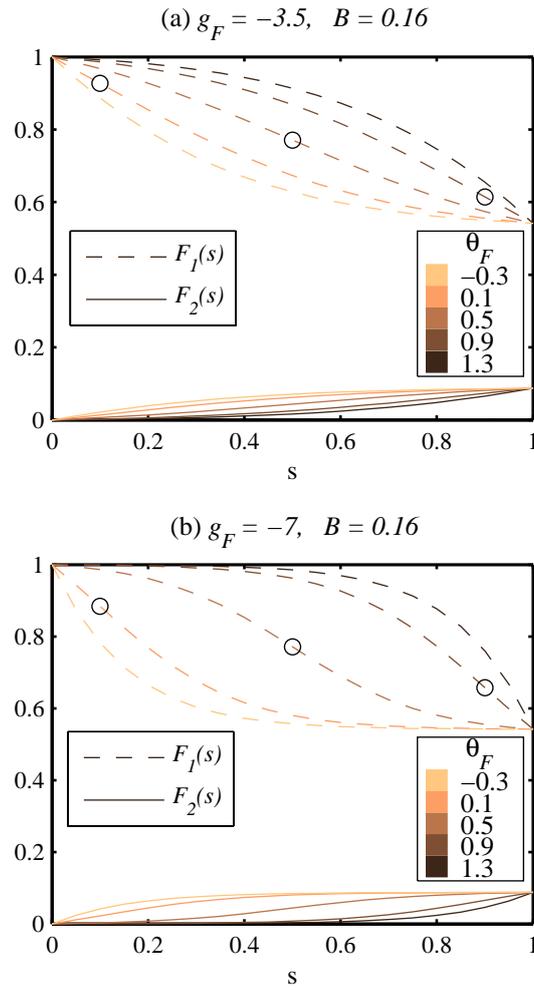
(Color online) Figure 2 : Influences of θ_F and g_F on weighting functions $F_1(s)$ and $F_2(s)$. These two functions determine the firing rate of excitatory population based on two competing terms $S_e^{prev}(h_e)$ and S_e^{mod}. Increment of s raises the firing rate by increasing/decreasing the value of $F_2(s)$ / $F_1(s)$. θ_F determines their convexities. If θ_F be smaller than zero, $F_1(s)$ and $F_2(s)$ are convex and concave functions respectively in the range of zero and $s^{\max}$. Convexities are reversed if θ_F is greater than $s^{\max}$. In between, these two functions have inflection points that have indicated on $F_1(s)$ by circles. g_F controls slopes of $F_1(s)$ and $F_2(s)$.
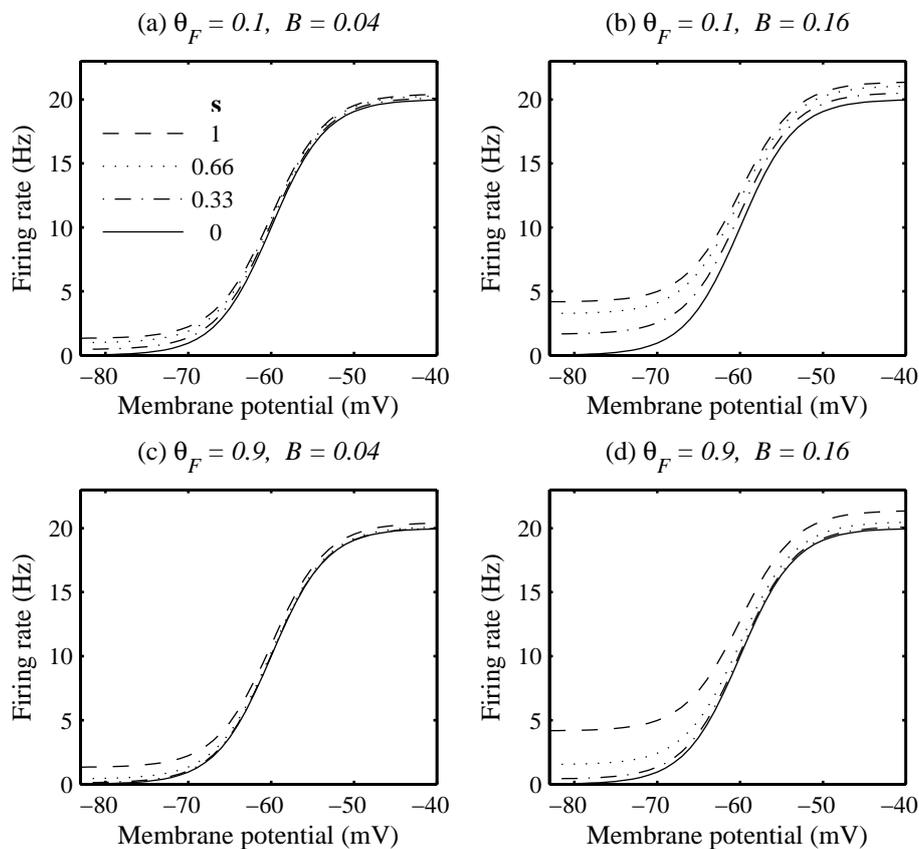
Figure 3 : Influences of s, θ_F and B on excitatory firing rate. Increase of s raises the firing rate value especially in low membrane potentials. Increasing the gain of modulating mechanism B from 0.04 to 0.16 (compare left and right figures) increases the influence of s on excitatory firing rate. θ_F does not change the value of excitatory firing rates at boundaries of s (i.e. at 0 and $s_\infty^{\max}$) but it can affect ascending shape of excitatory firing rates corresponding to $0 < s < s_\infty^{\max}$ (compare top and bottom figures).
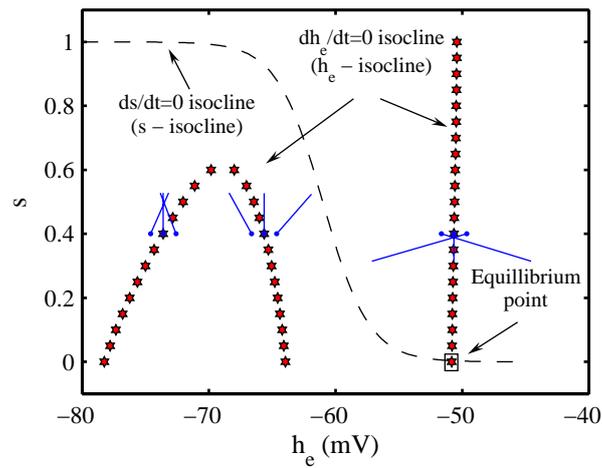
(Color online) Figure 4 : A typical $s-$ isocline (dashed line) and h_e- isocline (hexagrams) and nine candidate planar vectors. Origins of the vectors are located in $(s = 0.4, h_e^\bullet + \Delta h_e)$ where $\Delta h_e = \{-1, 0, +1\}$ mV and $h_e^\bullet$ is the equilibrium point of the model in a given s value (blue hexagrams). The intersection point of the two isoclines (s, h_e- isoclines) indicates the equilibrium point. Coordinates of this point indicate the equilibrium values of h_e and s. Convergent or divergent directions of vectors around a given point on h_e- isocline determine stability or instability status of that point.
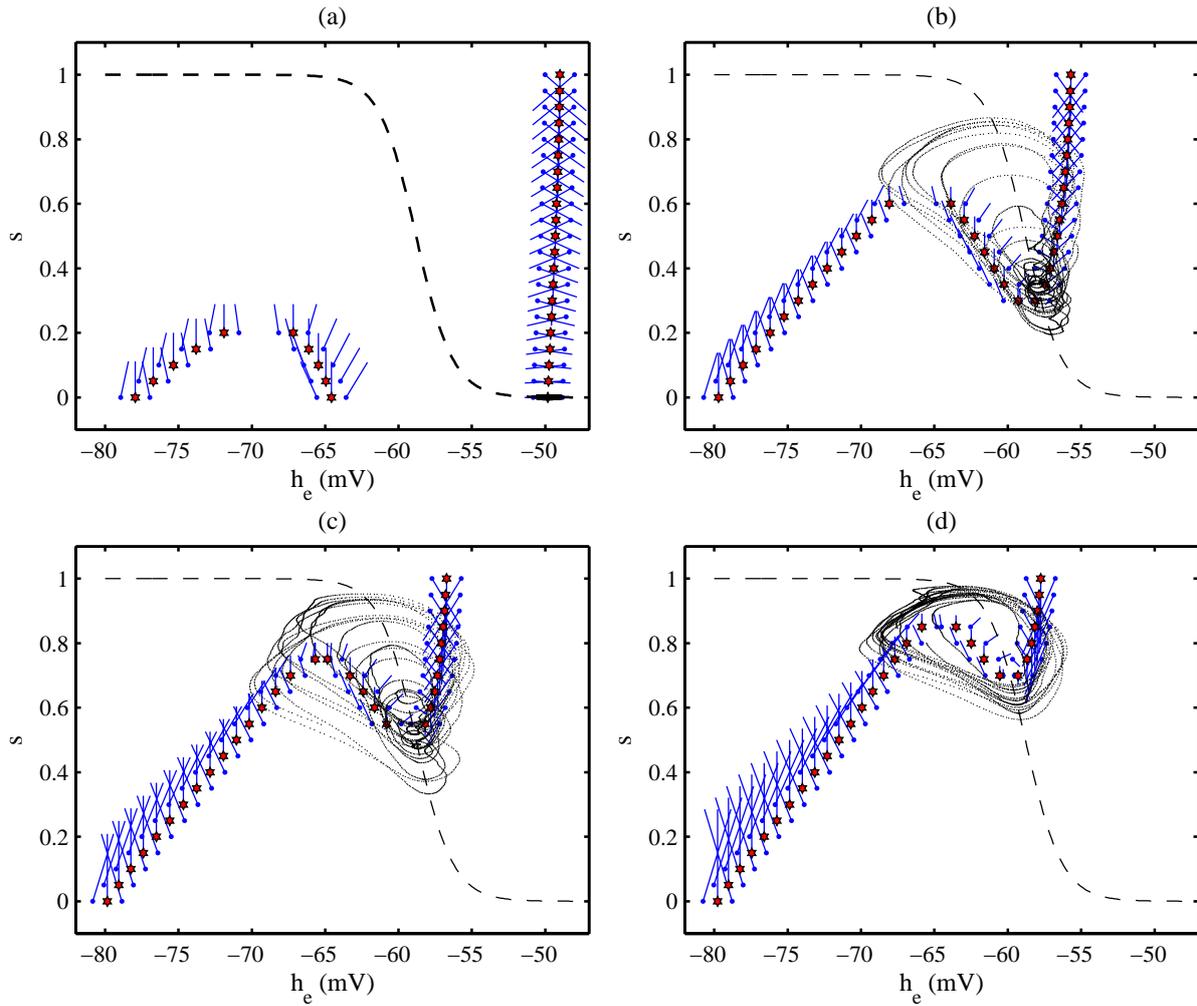
(Color online) Figure 5 : s, h_e − isoclines (dashed line and hexagrams) and 10-seconds (s, h_e) trajectories superimposed on them in different depth of anesthesia. Ordinates and abscissas of vectors (solid lines marked at vector origins) are proportional to the values of ds/dt and dh_e/dt respectively. (a) When drug concentration is low ($c = 0.2$ mM), $h_e(t)$ fluctuates about a stable equilibrium point. (b) When drug concentration increases to 0.75 mM, slow waves are appeared on background noisy fluctuations. (c) In $c = 0.9$ mM background noisy fluctuations are substituted with a more rhythmic activity. (d) When anesthetic concentration is set to 1.5 mM, the trajectory travels between up and down states regularly.
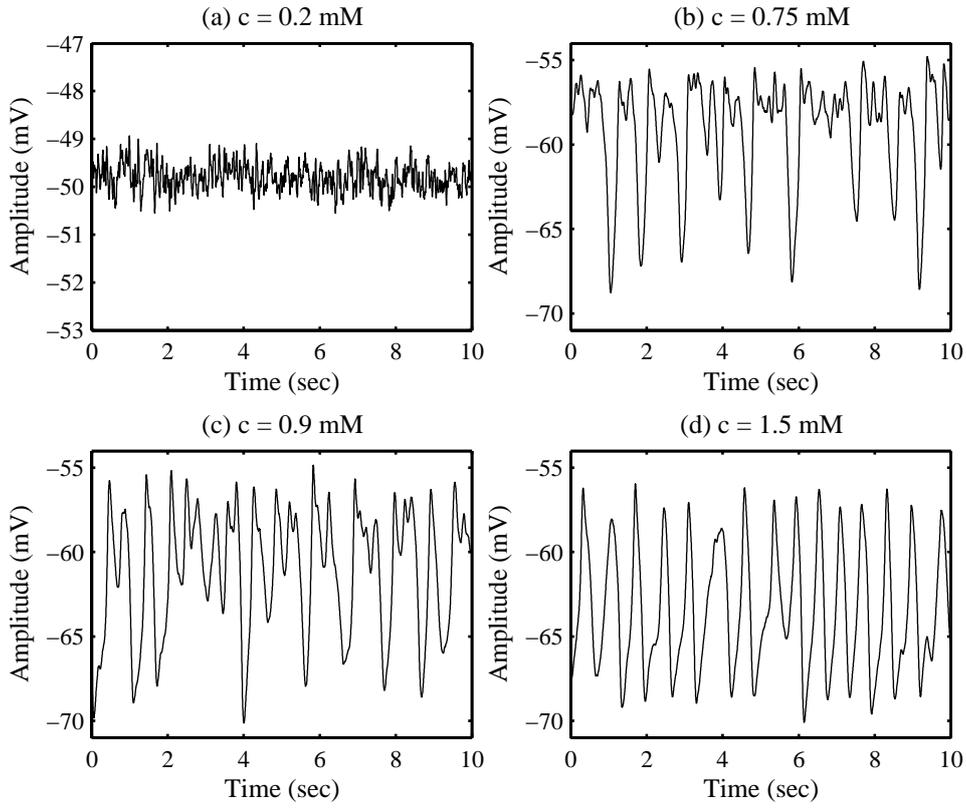
Figure 6 :   Ten seconds of simulated h_e signals in various anesthetic concentrations (0.2, 0.75, 0.9 and 1.5 mM). These signals correspond to illustrated trajectories in figure 5.
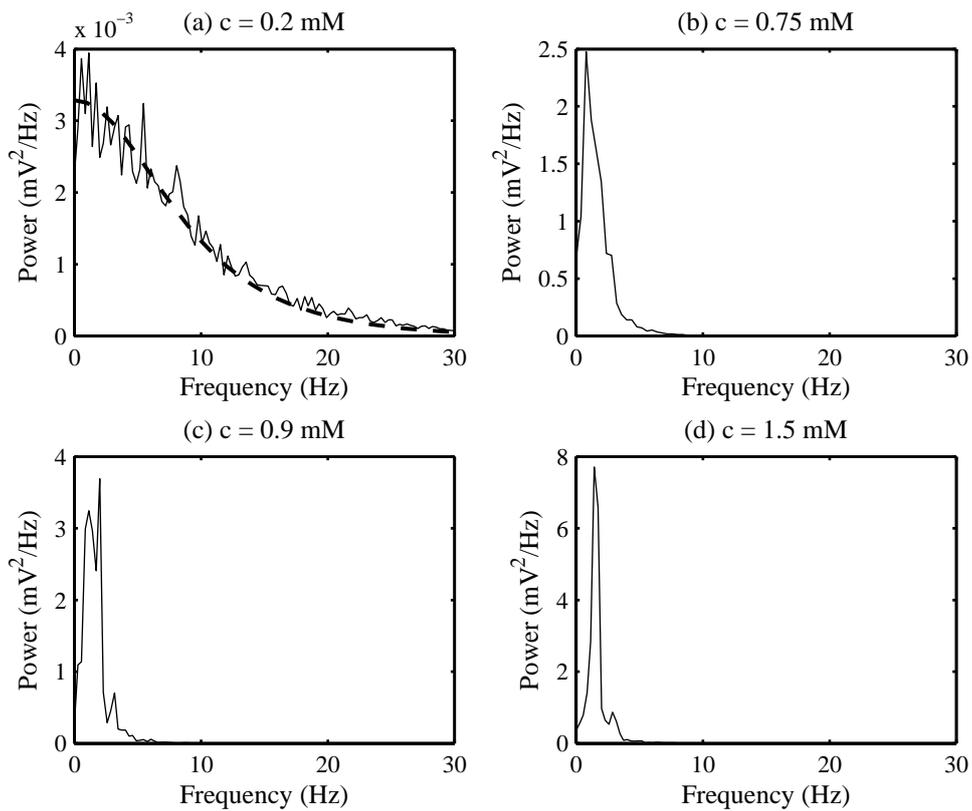
Figure 7 : The power spectra of simulated h_e signals in different drug concentrations. Each power spectrum is calculated by averaging 20 power spectra of consecutive 2.56 s h_e epochs (*i.e.* 51.2 sec). (a) In very low drug concentration ($c = 0.2$ mM), the power spectrum extends to high frequency terms. The eigenspectrum (dashed line) corresponding to this drug concentration is a descending function that reminiscent the background spectrum of a real EEG signal in waking period. (b) Appearance of slow waves ($c = 0.75$ mM), increases the energy of the slow delta band in the power spectrum. (c) Increasing the rate of slow waves ($c = 0.9$ mM) increases the energy of the fast delta band in the power spectrum. (d) Regular switching between up and down state ($c = 1.5$ mM) narrows the h_e spectrum in fast delta band.
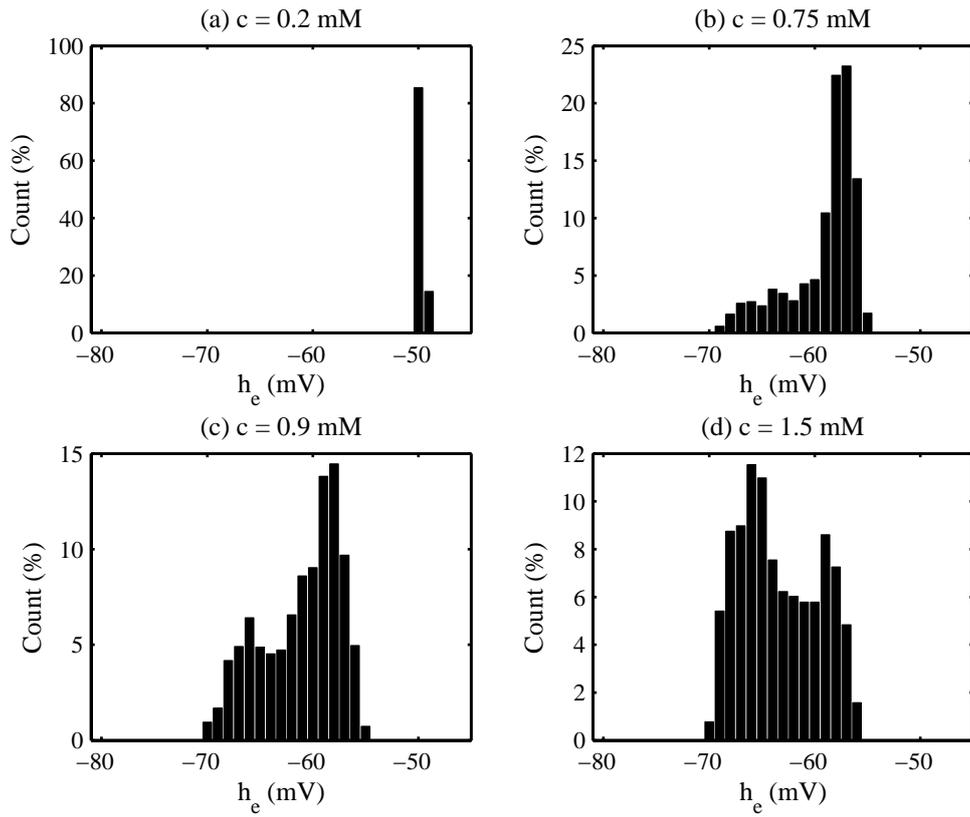
Figure 8 : Histograms of simulated h_e **signals in different anesthetic drug concentrations. (a) In very low drug concentration (** $c = 0.2$ **mM) the histogram contains only one peak centered in the up state area. (b) Slow waves extends the histogram to down state (** $c = 0.75$ **mM). (c) The histogram contains two peaks in up and down states (** $c = 0.9$ **mM). (d) The amplitude of the peak locating in down state may be equal or even higher than the amplitude of the other peak (** $c = 1.5$ **mM).**
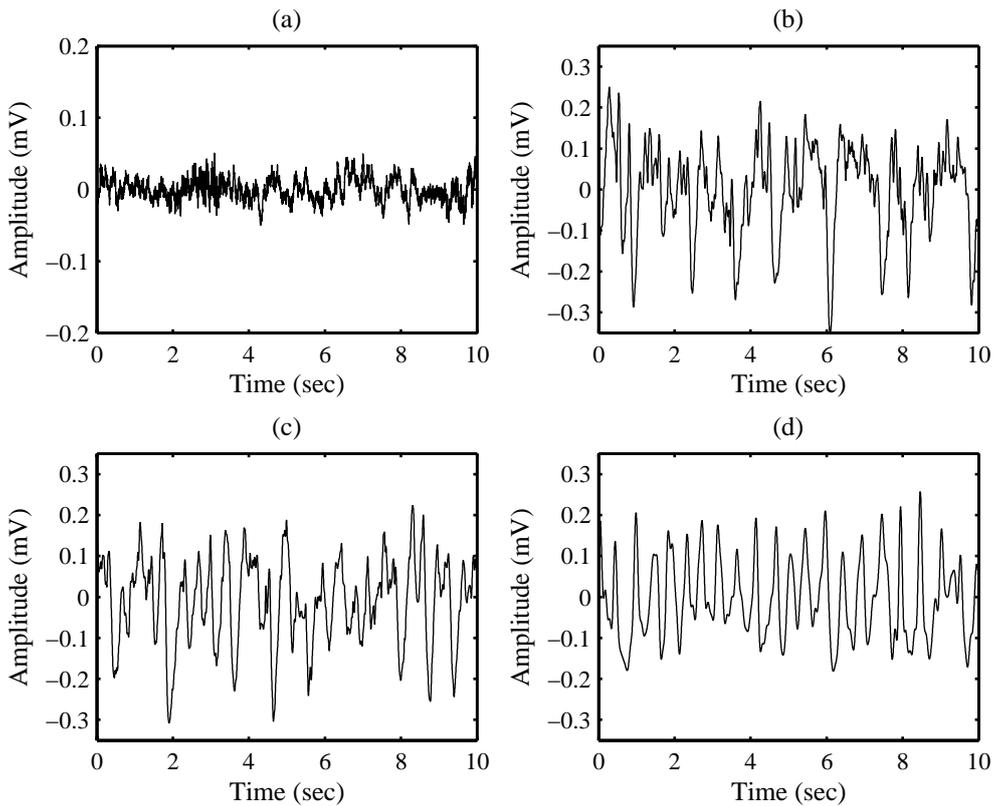
Figure 9 **: Real EEG signals recording on children undergoing surgery with Desflurane agent** [37]**. (a) EEG signal before administration of Desflurane. The patient is awake and eyes-open condition. (b) EEG signal at 1 MAC anesthesia. The high amplitude negative peaks are easily distinguished from high frequency lower amplitude background EEG activities. (c) The EEG at a concentration higher than 1 MAC. The number of negative peaks is increased in this signal and high frequency low amplitude background activities are replaced by lower frequency higher amplitude activities. (d) EEG signal at 2 MAC. This signal mainly consists of high amplitude rhythmic pulses.**
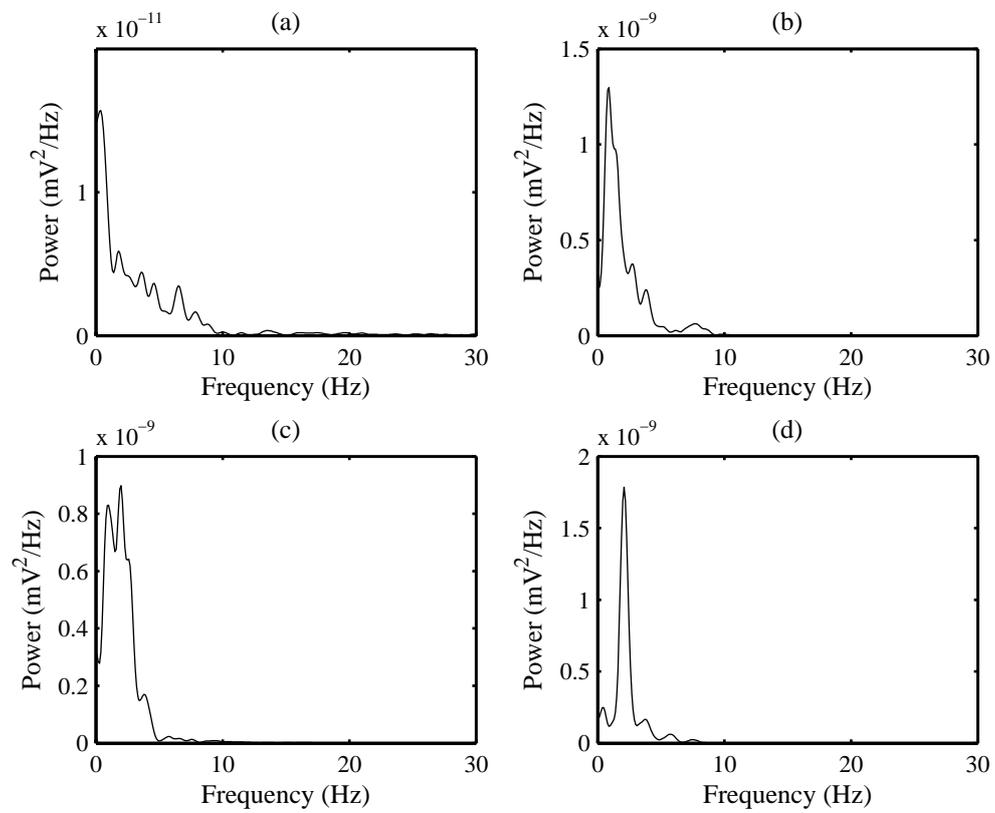
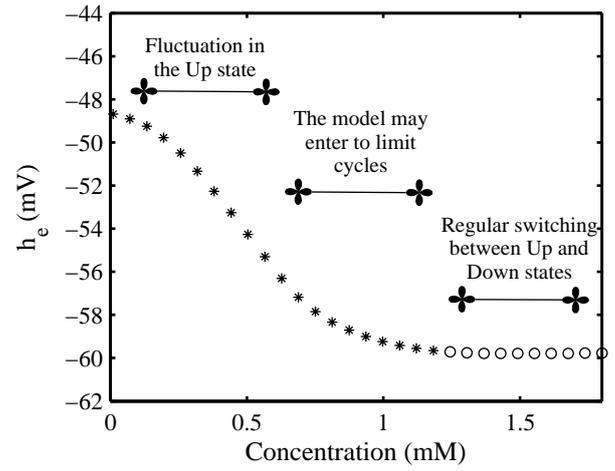**Figure 10 : Power spectrums corresponding to the illustrated real EEG signals in Figure 9.**
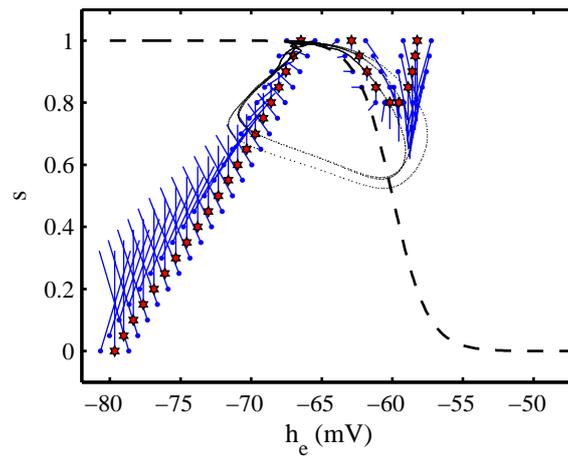
Figure 11 : Equilibrium solutions of h_e when anesthetic drug concentration is varied between 0 and 1.8 mM. Stars are stable and circles are unstable solutions of linear stability analysis.

(Color online) Figure 12 : s, h_e − **isoclines and a 20-second** (s, h_e) **trajectory corresponding to burst-suppression in high anesthetic drug concentration (** $c = 1.8$, $B = 0.14$, $\theta_s = -60$ **). The intersection of the two isoclines is very close to the saddle point of the** h_e − **isocline so** (s, h_e) **trajectory has the possibility of short-time traveling from down to up state.**
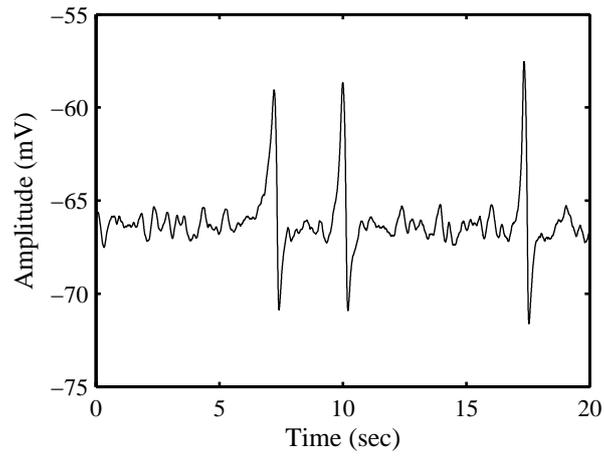
Figure 13 : Twenty seconds of simulated h_e signal corresponding to the illustrated (s, h_e) trajectory in Figure 12. This activity is reminiscent of burst-suppression activity in deep anesthesia.
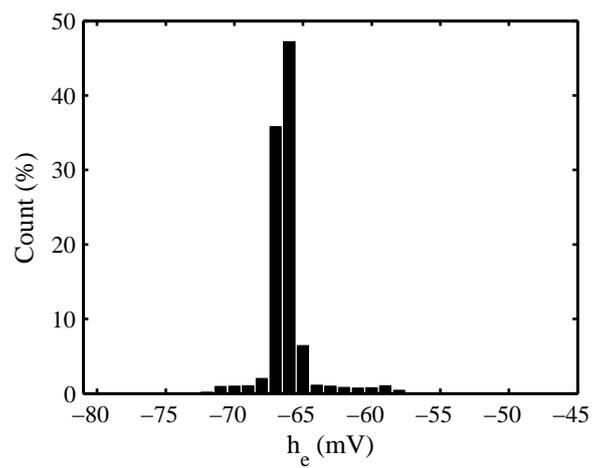
Figure 14 : The histogram of the depicted signal in Figure 13. The histogram only has one peak in down state area.
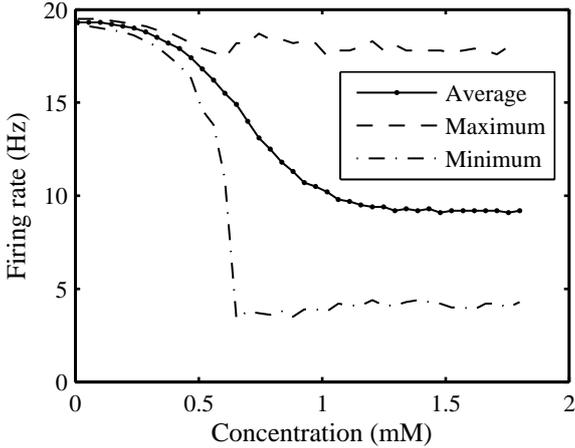
Figure 15 : Average and extremum values of excitatory firing rate in different drug concentrations. Firing rates are calculated based on numerical simulation of the model for 51.2 sec.

Parameter	Symbol	Value	Parameter	Symbol	Value
Mean resting membrane potential	$h_{e,i}^{rest}$	-77, -77 mV	Passive membrane decay time constant	$\tau_{e,i}$	45, 30 ms
Synaptic reversal potential	$h_{e,i}^{rev}$	0, -85 mV	Peak amplitude of EPSP/IPSP	$G_{e,i}$	0.3, 0.32 mV
EPSP/IPSP rate constant	$\gamma_{e,i}$	0.5, 0.15 ms^{-1}	Total number of $e \rightarrow e$, $e \rightarrow i$ local synaptic connections	$N_{ee,ei}^{\beta}$	2400, 2300
Total number of $i \rightarrow e$, $i \rightarrow i$ local synaptic connections	$N_{ie,ii}^{\beta}$	200, 440	Total number of synaptic connection from distant excitatory population	$N_{ee,ei}^{\alpha}$	2000, 1600
Spatial drop off rate of long-range excitatory connections	Λ	0.4 cm^{-1}	Mean axonal conduction speed	$\bar{v}$	0.7 cm ms^{-1}
Maximum firing rate	$S_{e,i}^{max}$	0.02, 0.02 ms^{-1}	Inflexion-point voltage for firing rate sigmoid function	$\theta_{e,i}$	-60, -60 mV
Firing rate sigmoid slope at inflexion point	$g_{e,i}$	0.3, 0.3 mV^{-1}	Subcortical mean firing rate	$\bar{p}_{ek}, \bar{p}_{ik}$	0.5, 0.4 ms^{-1}
weighting factors for fluctuations in $\bar{p}_{jk}$ spike inputs	α	1	Effective time constant of slow ionic currents	τ_s	180 ms
Slope at the inflexion-point of the activity function (sigmoid) of slow mechanism	g_s	-0.8 mV^{-1}	Inflexion-point voltage of the activity function (sigmoid) of slow mechanism	θ_s	-58.8 mV
Maximum value of the activity function (sigmoid) of slow mechanism	S_{∞}^{max}	1	Slope at the inflexion-point of the modulating sigmoid function	g_F	-3.5
Inflexion-point of the modulating sigmoid function	θ_F	0.1	Maximum firing rate due to the modulating mechanism.	S_e^{mod}	0.03 ms^{-1}
Gain of the modulating mechanism	B	0.16			

Table 1: Symbol definitions and constants values of the enhanced model